Universiteit
Leiden
The Netherlands

Charge transport properties of Ru-complex molecules: the influence of humidity

Atesci, H.

Citation

Atesci, H. (2019, December 3). *Charge transport properties of Ru-complex molecules: the influence of humidity. Casimir PhD Series*. Retrieved from https://hdl.handle.net/1887/81089

Version:	Publisher's Version
License:	Licence agreement concerning inclusion of doctoral thesis in the Institutional Repository of the University of Leiden
Downloaded from:	https://hdl.handle.net/1887/81089

Note: To cite this publication please use the final published version (if applicable).

Cover Page

Universiteit Leiden

The following handle holds various files of this Leiden University dissertation:
http://hdl.handle.net/1887/81089

Author: Atesci, H.
Title: Charge transport properties of Ru-complex molecules: the influence of humidity
Issue Date: 2019-12-03

Appendix

A.1 XPS characterization

The surface composition of bare ITO and Ru-complex SAMs on ITO samples were analyzed by X-ray photoelectron spectroscopy (XPS). Figure A.1 displays XPS spectra of bare ITO, and for a layer of **2-Ru-N** complex molecules assembled on ITO. Bare ITO electrode shows a peak around 530 eV with a small shoulder around 533 eV indicating the presence of oxygen on the surface. From XPS peak analysis, we estimated the total amount of detectable surface oxygen (present as "OH") to be 26%. In the C(1s) region, a broad peak between 284 and 287 eV is observed. It is identified as a carbon 1s signal originating from the Ru complex. At the lower binding energy region near 281 eV, a small signal originates from a Ru3d5/2 peak, observed for the **2-Ru-N**/ITO Sample. The peak around 400 eV, present for **2-Ru-N**/ITO, but absent for ITO only, is assigned as N1s signal in the Ru complex. In addition, a broad peak around 133 eV is assigned as P2p signal in the Ru complex. These XPS data confirm the immobilization of the **2-Ru-N** complex on ITO electrode involving bidentate/tridentate binding through P–O–In and/or P–O–Sn bonds(*67*).

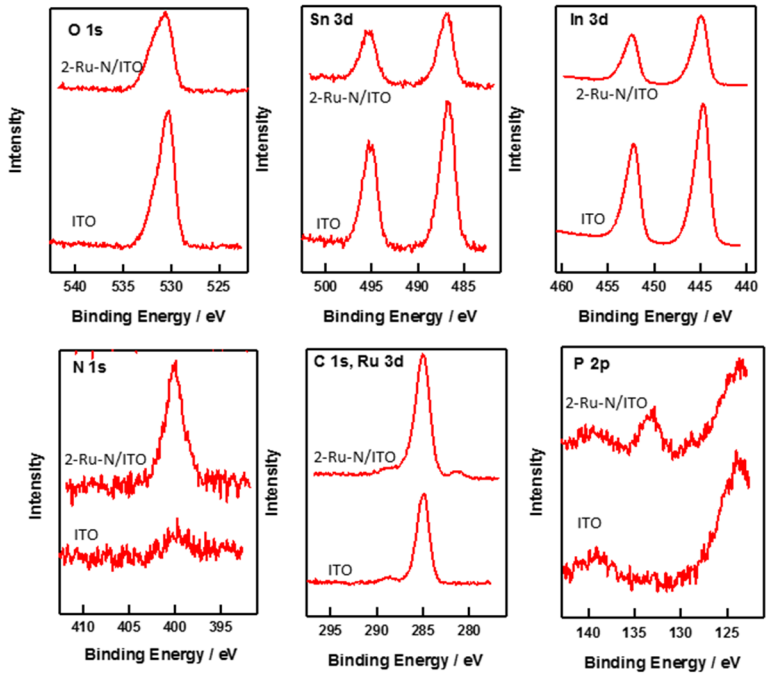

Figure A.1: X-ray photoelectron spectra of bare ITO and **2-Ru-N** SAM on ITO in the narrow region of O 1s, Sn 3d, In 3d, N 1s, C 1s , Ru 3d and P 2p. Complete range XPS data is shown in the supporting information in the following publication by Kaliginedi *et al.*(*67*).

A.2 AFM molecular height characterization

Due to relatively high surface roughness of the ITO substrate compared to the height of the molecular layer, estimating the molecular length on the surface from the AFM image profile will lead to relatively large errors. To exclude the contribution of surface roughness as much as possible, an AFM scratching experiment was performed by Kaliginedi *et al.* on an ultra-flat sapphire (Al_2O_3) substrate, which binds to phosphonate linker group of the Ru complex as efficiently as ITO. In this case, **2-Ru-N** is shown as an example in Figure A.2a, where an AFM image of the **2-Ru-N** molecules are shown after the immersion of the sapphire substrate into the **2-Ru-N** solution (1 μM) for 1 min. The bright spots seen in Figure A.2a indicate the presence of the molecule on the surface, these being absent on the bare sapphire surface. Molecular dots with almost the

same average height of ≈2 nm are scattered over the surface (Fig. A.2b). The observed height is consistent with the molecular model of the **2-Ru-N** complex with vertical orientation as shown in Fig. A.2c. These measurements are in good agreement with the theoretically predicted molecular length, confirming the vertical orientation of the molecule on the electrode surface(*67*). This indicates that the bottom four phosphonic acid groups of the tetrapodal anchoring groups attach to the ITO electrode via bidentate/tridentate binding through P–O–In and/or P–O–Sn bonds. A point worth noting is the rather high force, approximately 3.4 µN that was required to scratch off the molecular layer from the surface, which is 2 orders of magnitude higher than the C-AFM measurements presented in this thesis. This indicates the very strong bonding of phosphonic acid anchoring groups on ITO surface.

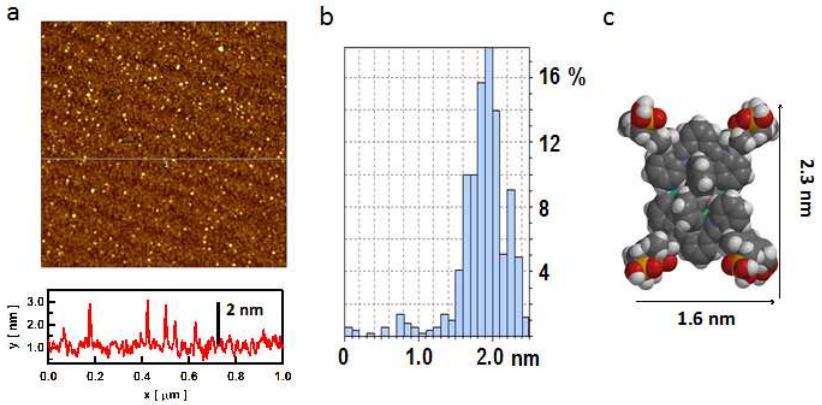

Figure A.2: AFM images of the **2-Ru-N** molecules immobilized on sapphire substrate (a) from low concentration and short immersion time (1 µM for 1 min). Height distribution calculated from the AFM image (b). CPK model of the **2-Ru-N** molecule with molecular length indicated (c). This data is previously reported in the SI of in the following publication(*121*).

A.3 AFM surface topography characterization

Topographical AFM images were acquired using tapping mode in ambient conditions on freshly prepared samples of bare ITO, and monolayers of **1-Ru-N**, **1-Ru-Py** and **2-Ru-N** (we lack images of **2-Ru-N-dec**, and **2-Ru-C**). We scanned a 3×3 µm area and included a line section over distances of ≈1 µm. The surface of bare ITO shows relatively flat grains with sizes of up to few hundreds of nm, which are separated by trenches and holes. The trenches are typically 2-3 nm deep, the hole depths vary between 5 and 8 nm. The images do not permit to recognize any ordered layer of molecules on the ITO surface.

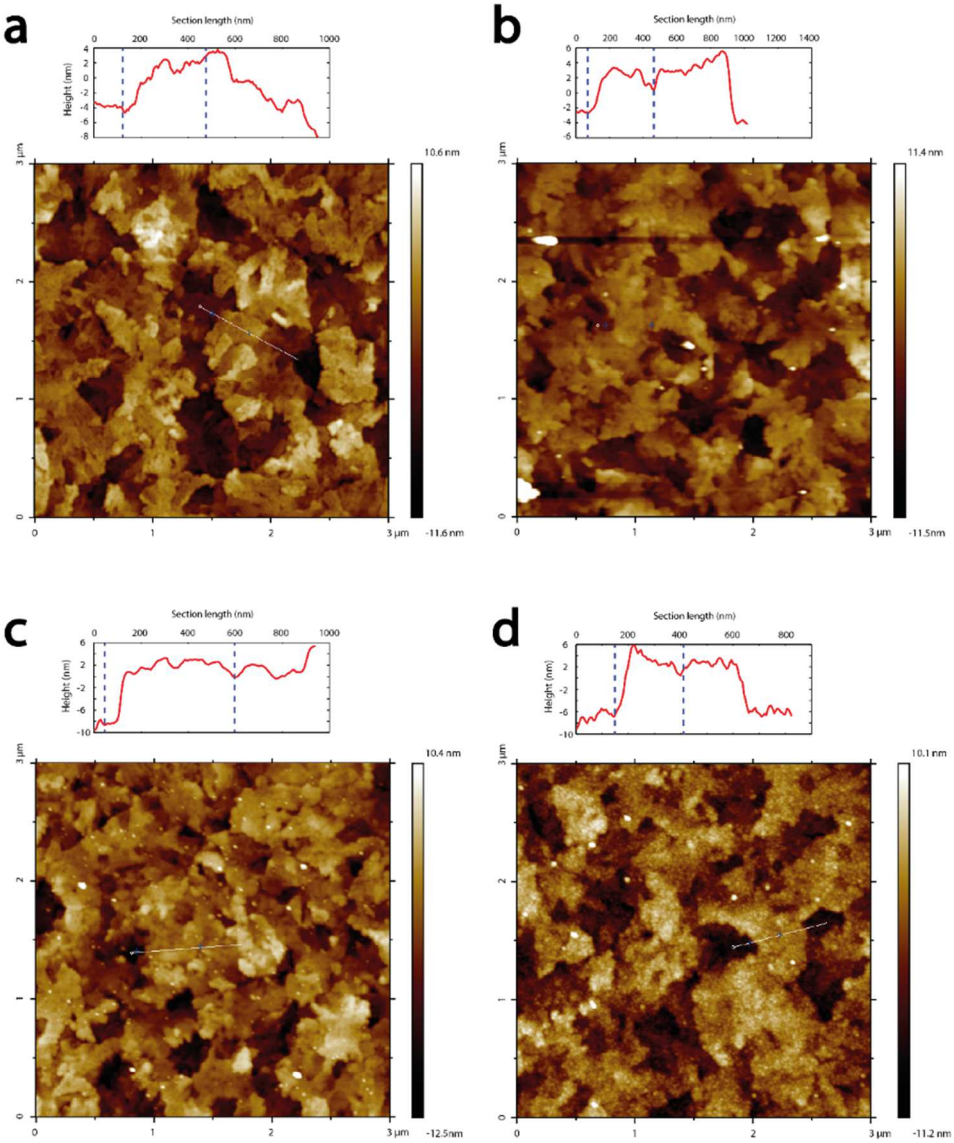

Figure A.3: Topography images on 3×3μm areas made with tapping mode AFM on RCA treated and Ar ion beam etched ITO (a), on top of which is grown 1 monolayer of **1-Ru-N** (b), **1-Ru-Py** (c), and **2-Ru-N** (d). The respective line scans are shown on top of the images.

A.4 Tip-radius-dependent measurements for 2-Ru-N at high humidity

We have looked into the tip radius dependency of the I-V characteristic of **2-Ru-N** under humid conditions with a Au top contact, while keeping the pressure (as seen in Fig. A.4a, which is derived from the theoretical work of Carpick *et al.*(*71*)) as equal as possible for all cases. The results from Fig. A.4b-d show that there is indeed inverse relation between the RR at 0.9V and tip radius.

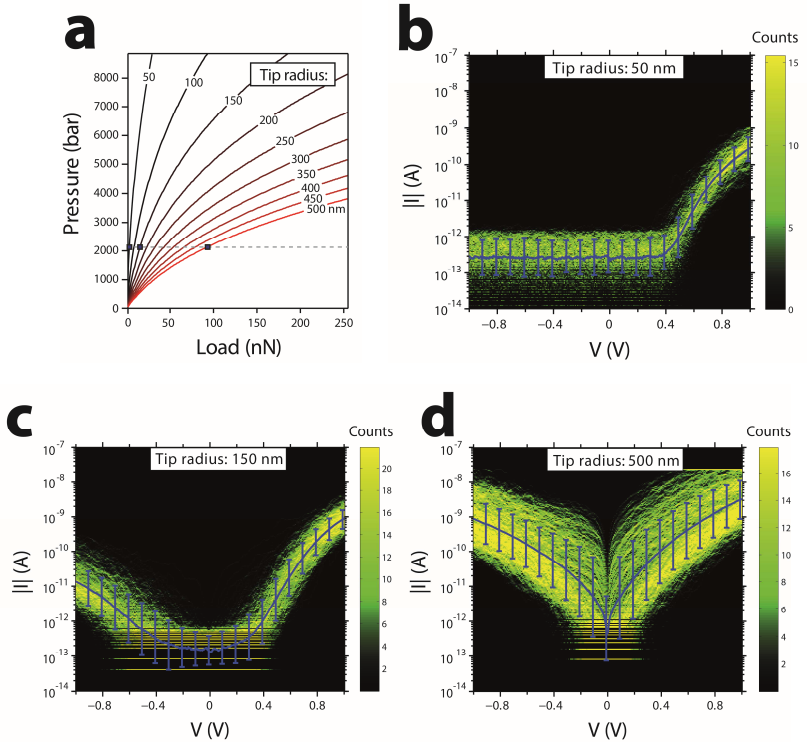

Figure A.4: Theoretical curves of the pressure on the SAM versus tip load with varying tip radii. The parameters and formulae used for this approximation is derived from the following paper from Carpick *et al.*(*71*). From the force values extracted from a), we performed tip radius dependent measurements while keeping the calculated pressure values constant (approximately 2100 bars) for all tip radii. Tip radius dependent |I|-V measurements with their corresponding RR-V plots of **2-Ru-N** junctions humid conditions measured with three different AFM tip radii: 50 (b), 150 (c) and 500 nm (d) with a corresponding force set point of 1 nN, 10 nN and 90 nN, respectively. A Gaussian was used to fit the data set at each voltage bin, with the mean values shown in the colored lines. The error bars follow from the half widths of the Gaussian fits. Note that in all cases the tip radii were independently confirmed using scanning electron microscopy.

A.5 Transport measurements on bare ITO

We have measured the I-V characteristics of the bare ITO substrate with a ITO top contact in both dry and humid conditions, the results of which can be seen in Fig. A.5.

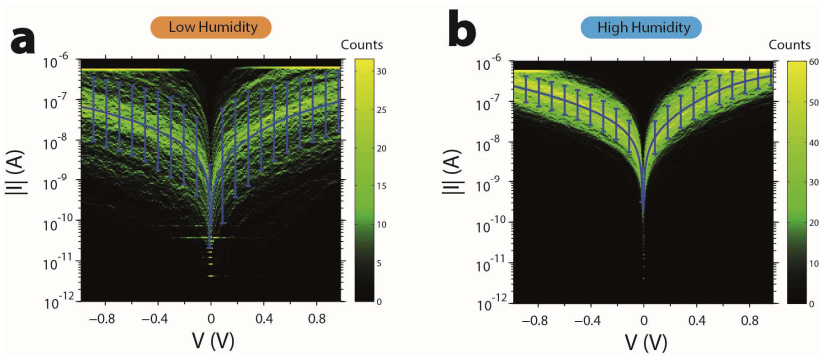

Figure A.5: The 2D-histogram of logarithmically binned |I|-V characteristics of the bare ITO-ITO junction are shown for low humidity (a) and high humidity (b) conditions. Overlaid in blue is the mean of the Gaussian fits at each bias voltage bin. The error bars follow from the half widths of the fits.

We have also measured the I-V characteristics of the bare ITO substrate with a Au top contact in both dry and humid conditions, see Fig. A.6.

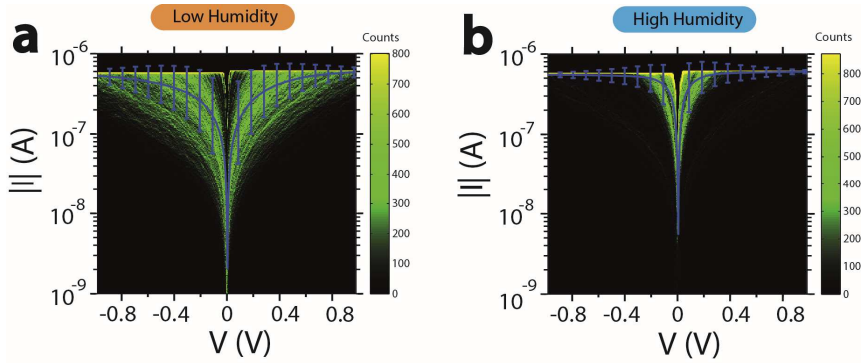

Figure A.6: The 2D-histogram of logarithmically binned |I|-V characteristics of the bare Au-ITO junction are shown for low humidity (a) and high humidity (b) conditions. Overlaid in blue in (a,b) are the means of the Gaussian fits at each bias voltage bin. The errorbars follow from the half widths of the fits.

A.6 Temperature-dependent measurements for 2-Ru-N in humid conditions

We have also performed I(V,T) measurements at high humidity (see Fig. A.7a). Unfortunately, these data cannot be straightforwardly interpreted. The reason is experimental: we set the relative humidity for the *entire chamber*, whilst we change the temperature of the sample only *locally*. As a result, the humidity value $h_s(T)$ just around the heated sample is much smaller than the global value $h_c(T)$ in the chamber. Since we know that RR depends strongly on (local) humidity, this effect should be taken into account. We anticipate RR (T; $h_c(T)$), i.e. we allow for both an intrinsic T-dependence of RR (the result wanted), and an indirect dependence via the temperature-dependence of the local humidity. To calculate the effect of the latter, we first compute the values that h_s assumes for the four temperatures considered (60%, 30%, 14%, and 7% respectively), from the change in the water vapor pressure with temperature. For these humidity values, we inspect the RR(V) curves measured at room temperature, shown in Fig. A.7b, and determine the RR values at 0.9 V. These are then plotted in Fig. A.7c, together with the RR values determined from Fig. A.7a. Interestingly, these data sets match very well. In other words, we can explain the full temperature-

dependence found for RR from local changes in humidity, without needing an intrinsic temperature-dependence, within our error bars.

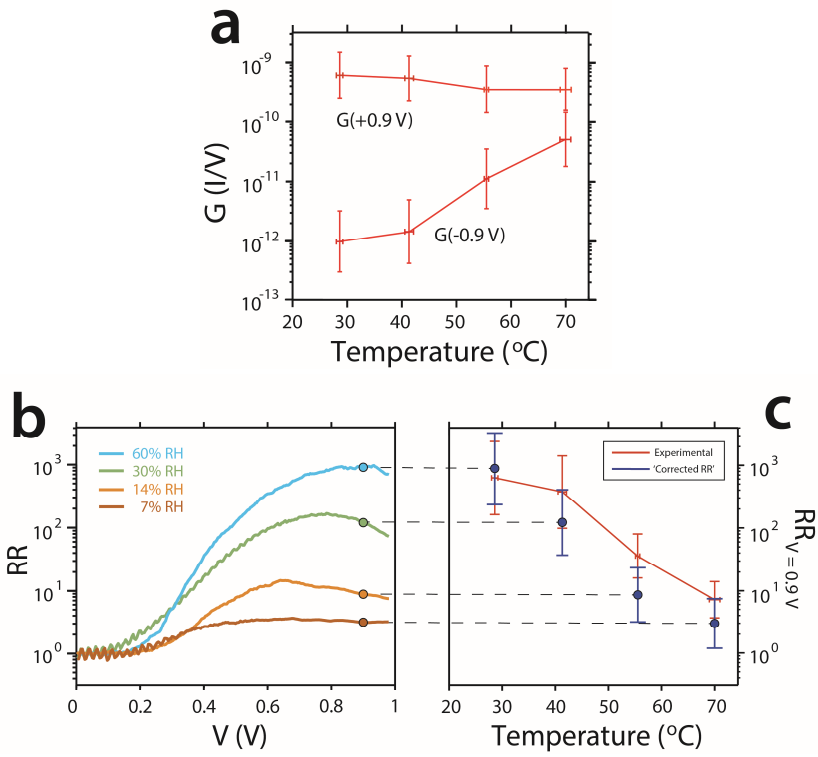

Figure A.7: (a) Conductance measured for **2-Ru-N** junctions at high humidity values $h_c \approx 60\%$ (defined for the full chamber), as a function of sample temperature, for +0.9 V and -0.9 V. In (c), the RR-values (red) as determined from (a) are shown vs temperature. However, these experimental data are influenced by the fact that the local relative humidity around the sample (h_s) will strongly decrease as the sample temperature is increased. Lower local humidity will directly influence RR. To try to correct for this effect, we take the h_c value at room temperature and estimate the partial pressure ($p_{28°C}$) of water in the chamber. We then assume $p_{28°C}$ to stay constant during the course of the measurements (NB the gas volume around the tip is relatively small). As the sample is heated, the local water vapor pressure increases and the local relative humidity h_s decreases inversely to that, as $p_{28°C}$ stays the same for the full chamber. With the known psychrometric charts, we calculate h_s at the relevant temperature values, yielding 60%, 30%, 14%, and 7% for 28°C, 40°C, 55°C, and 70°C, respectively. Next, we make the assumption that the full temperature-induced effect on RR is via changes in $h_s(T)$. This allows us to connect to Fig. (b), which shows the RR vs. V curves that we have measured at the relevant humidity values at room temperature. From (b), we extract RR values at 0.9 V, which we replot in (c), but now as a function of 'temperature'. The latter means that we e.g. connect 7% humidity to 70°C , etc. The resulting data set, called 'Corrected RR', is plotted in blue in (c). We find that the measured change in RR values matches this 'Corrected RR' data, within the error bars. Thus, our RR(T) data can be almost fully attributed to a change in h_s without the need to assume an explicit temperature-dependence of the conductance, within error bars. NB these are data obtained with a Au-tip, for a SAM on ITO.

A.7 Details on the Fermi-distribution-broadening calculations

The temperature dependence for the two-site coherent model was obtained from our quantum chemistry calculations in dry conditions. We have considered a two-site model where the chemical potentials are both E_0 with respect to the chemical potential of the electrodes at V=0, with a broadening $\Gamma=\Gamma_R+\Gamma_L$. Where Γ_L is the tunnel rate to the left electrode and Γ_R to the right electrode. In this model the temperature is included through of the Fermi distribution function(*123*). Figure A.8 shows the results of the calculated current as a function of the inverse of the temperature at different bias voltages normalized to E_0. At low temperatures, the current is temperature-independent. As the temperature increases, the tails of the

Fermi distributions of the electrochemical potentials start to overlap with the energy levels increasing exponentially with temperature.

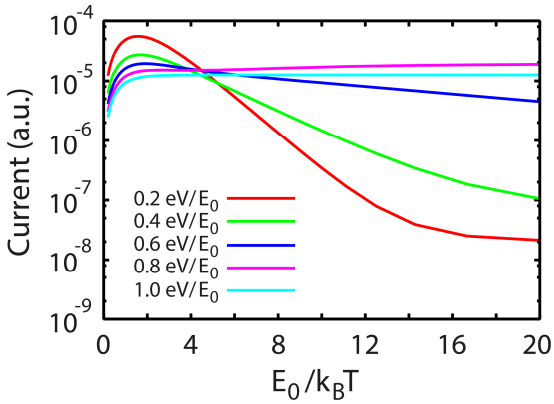

Figure A.8: Calculated current as a function of the inverse temperature for five different bias voltages for a broadening $\Gamma = 0.002E_0$.